Journal of Rock Mechanics and Geotechnical Engineering 14 (2022) 653–662

Contents lists available at ScienceDirect

Journal of Rock Mechanics and Geotechnical Engineering

journal homepage: www.jrmge.cn

Technical Note

Effects of water saturation and loading rate on direct shear tests of andesite

Tianshu Bao*, Kimihiro Hashiba, Katsunori Fukui

Department of Systems Innovation, The University of Tokyo, Tokyo, 113-8656, Japan

ARTICLE INFO

Article history:
Received 7 February 2021
Received in revised form
31 March 2021
Accepted 17 July 2021
Available online 16 September 2021

Keywords:
Direct shear test
Water saturation
Loading rate dependence
Failure criterion

ABSTRACT

For estimating the long-term stability of underground framework, it is vital to learn the mechanical and rheological characteristics of rock in multiple water saturation conditions. However, the majority of previous studies explored the rheological properties of rock in air-dried and water saturated conditions, as well as the water effects on compressive and tensile strengths. In this study, andesite was subjected to direct shear tests under five water saturation conditions, which were controlled by varying the wetting and drying time. The tests were conducted at alternating displacement rates under three vertical stresses. The results reveal that the shear strength decreases exponentially as water saturation increases, and that the increase in shear strength with a tenfold increase in displacement rate is nearly constant for each of the vertical stresses. Based on the findings of the shear tests in this study and the compression and tension tests in previous studies, the influences of both water saturation and loading rate on the Hoek-Brown failure criterion for the andesite was examined. These results indicate that the brittleness index of the andesite, which is defined as the ratio of uniaxial compressive strength to tensile strength, is independent of both water saturation and loading rate and that the influences of the water saturation dependence and the loading rate dependence of the failure criterion can be converted between each other.

1. Introduction

To estimate the long-term stability of underground constructions, it is necessary to consider the mechanical and rheological characteristics of rock. Water is widely recognized as one of the major influencing factors on the deformation and failure of intact rock (Kirby, 1984). Several studies have revealed that uniaxial compressive strength (Dyke and Dobereiner, 1991; Vásárhelyi and Ván, 2006; Talesnick and Shehadeh, 2007), uniaxial tensile strength (Hawkes et al., 1973; Ojo and Brook, 1990; Hashiba and Fukui, 2015), and Brazilian tensile strength (Gunsallus and Kulhawy, 1984; Talesnick et al., 2001; Erguler and Ulusay, 2009) are lower in wet conditions than in dry conditions. Although these studies focused on only wet and dry conditions, Hashiba et al. (2019) and Bao et al. (2021) researched the uniaxial compressive and Brazilian tensile characteristics of rock in various situations of water saturation and clarified the relationship between the water saturation and the strength. The stress corrosion reaction is considered to be one of the main water effects on strength and the time-dependent behavior of rock. As a time-dependent behavior, it is generally known that as the loading rate increases, the rock strength will be elevated (Brace and Martin III, 1968; Peng, 1973). For instance, the uniaxial compressive strength, the uniaxial tensile strength, and the shear strength of Sanjome andesite in dry conditions increase by 4.8 MPa (Hashiba et al., 2019), 0.42 MPa (Fukui et al., 2003), and 1.2 MPa (Fukui et al., 2004) on average, respectively, with a tenfold rise in loading rate. Hashiba et al. (2019) reported that the increase of the uniaxial compressive strength of Sanjome andesite with a tenfold rise of loading rate is virtually constant for various water saturation conditions. Here, the loading rate indicates the stress rate, strain rate, or displacement rate (Hashiba et al., 2018).

In terms of the shear strength of rock, previous research revealed the influence of water on the fracture friction angle and shear strength of discontinuous surfaces (Gutierrez et al., 2000; Li et al., 2005; Pellet et al., 2013; Ulusay and Karakul, 2016; Kim and Jeon, 2019). However, few investigations have been performed on

* Corresponding author.
E-mail address: fxbaoo@gmail.com (T. Bao).
Peer review under responsibility of Institute of Rock and Soil Mechanics, Chinese Academy of Sciences.

https://doi.org/10.1016/j.jrmge.2021.07.008

the shear characteristics of intact rock under different water saturation conditions, or the relationship between the water saturation dependence and the loading rate dependence, both of which are critical for understanding the rock failure criteria and determining the long-term stability of underground constructions. In this study, direct shear tests were conducted using Sanjome andesite under various water saturation conditions, and the effects of water saturation and loading rate on the shear strength were studied. In addition, by adopting previous data from compression tests (Okubo et al., 1990) and tension tests (Bao et al., 2021), the failure criterion and the relationship between the water saturation dependence and the loading rate dependence were discussed.

2. Rock specimens and experimental method

Sanjome andesite was used in this study. The groundmass of this andesite comprises hypersthene, augite, plagioclase, and magnetite phenocryst with the particle size ranging from 0.3 mm to 1.5 mm. The specimens are cylindrical in shape, with a diameter of 50 mm and a height of 50 mm, which were taken from an intact rock block. The porosity of this andesite is 19.7%. The uniaxial compressive strength and the Young's modulus of Sanjome andesite obtained from previous studies are listed in Table 1 (Okubo et al., 1990; Fukui et al., 2004; Bao et al., 2021). This investigation employed the same rock block of Sanjome andesite as the study in Fukui et al. (2004). Here, the uniaxial and triaxial compressive results of Okubo et al. (1990) and the Brazilian tensile results of Bao et al. (2021) will be subjected to the section of Discussion. And Bao et al. (2021) conducted the Brazilian tension tests under various water saturation conditions as in this study.

Fig. 1 illustrates the procedure for changing the water saturation conditions of specimens. After drilling, cutting, and polishing, all specimens were air-dried in the laboratory at 23 °C for over two weeks before being dried in an oven at 105 °C for 10 d until the mass of the specimens would remain constant. The minimum mass of each specimen during drying was recorded as m_d. Following this procedure, all the specimens were taken out of the oven and placed into a vacuum tank for 1 d. Then, they were immersed in deionized water and held for 10 d. Each mass of water-saturated specimen was measured as m_w. Some of the water-saturated specimens were subjected to direct shear tests with water saturation w of 1. In addition, two of the remaining specimens were submitted to the tests after being air-dried for 1 d. The water saturation w calculated via the following equation was 0.47 or 0.45:

$$w = \frac{m_i - m_d}{m_w - m_d} \quad (1)$$

where m_i is the mass of each specimen just before tests.

To achieve the different water saturation conditions, the remaining specimens were air-dried in the laboratory for one week or two weeks. The water saturation reached 0.14–0.17 and 0.045–0.046 after one-week drying and two-week drying, respectively, and then the tests were conducted. After these procedures, the remaining specimens were oven-dried for another 10 d. Then, some specimens were cooled in a sealed box filled with desiccant for over 12 h until they would be cooled to room temperature. These specimens were tested with a water saturation of 0.0025–0.0081, which was the lowest water saturation in this study. The remaining specimens were air-dried for around one week in the laboratory to increase the water saturation. After the water saturation reached 0.031–0.045, the tests were conducted with these specimens. This water saturation condition is labeled as low air-dried 2, which is different from the above-mentioned condition with air drying for two weeks (low air-dried 1). As it turned out, the test results were affected by the water saturation but not by these processes. The five water saturation conditions are shown in Table 2: extremely-dried, low air-dried 1 and 2, high air-dried, air-dried for 1 d, and water-saturated conditions.

Table 1
Mechanical properties of Sanjome andesite.

Reference	Uniaxial compressive strength (MPa)	Young's modulus (GPa)
Okubo et al. (1990)	92	10.2
Fukui et al. (2004)	94.7	10.2
Bao et al. (2021)	94.6	11.2

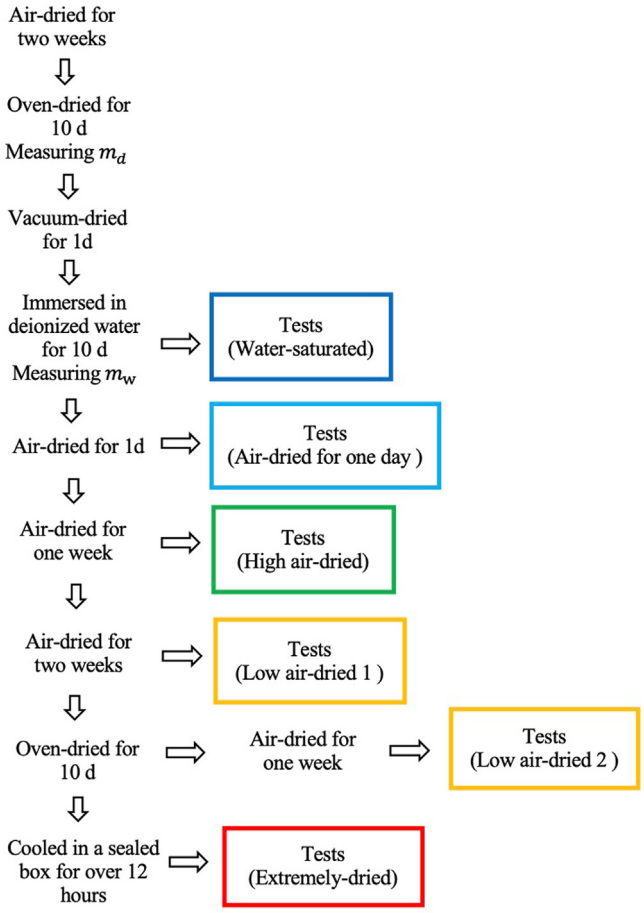

Fig. 1. Pregr13paration process for different water saturation conditions before the direct shear tests.

A 500 kN servo-controlled biaxial loading machine was used for the direct shear tests. Fig. 2a shows a schematic of the machine and the control system. The horizontal and vertical displacements of the loading platens were measured with two linear variable differential transformers (LVDTs). The horizontal and vertical loads were measured with two strain-gauge type load cells. The output signals of these measurement devices were delivered to the amplifiers and then to the computer through an analog to digital (A-D) converter. The loading part of the machine is shown in Fig. 2b. The horizontal and vertical loads were transmitted to the shear box via the bearing for avoiding the bending moment.

In the tests, the vertical load kept constant, and the vertical stress was determined by dividing the vertical load by the initial cross-sectional area of the specimen. The specimen was placed in the shear box, as shown in Fig. 2c, and the initial cross-sectional

Table 2
Experimental conditions and results of direct shear tests.

No.	Vertical stress (MPa)	Condition	Water saturation	Shear strength (MPa)	Residual strength (MPa)
25	10	Extremely-dried	0.004	27.4	7.6
22		Extremely-dried	0.0042	28.9	7.6
45		Extremely-dried	0.0047	29.5	9.6
23		Low air-dried 2	0.031	28.2	9.5
31		Low air-dried 1	0.046	26.8	8.6
10		High air-dried	0.14	22.8	8.6
39		High air-dried	0.16	23.8	7.9
15		High air-dried	0.17	26.9	9.9
41		Air-dried for 1 d	0.47	21.5	7.6
35		Water-saturated	1	22.3	8.6
33		Water-saturated	1	23.2	9.9
46	25	Extremely-dried	0.0025	48.8	20.9
47		Extremely-dried	0.0029	50	22.3
29		Extremely-dried	0.0041	51.2	24.3
43		Low air-dried 2	0.037	48.3	20.6
44		Low air-dried 2	0.039	50.6	23.2
27		Low air-dried 2	0.044	48.8	24.1
12		High air-dried	0.16	44.3	22.7
17		High air-dried	0.16	39.2	25.8
11		High air-dried	0.17	44.9	22.7
19		Water-saturated	0.99	39.9	21.4
38		Water-saturated	1	37.9	18.8
37		Water-saturated	1	39.6	24.5
26	40	Extremely-dried	0.0037	66.8	40.1
30		Extremely-dried	0.0038	67.2	35.5
48		Extremely-dried	0.0048	64.6	39.3
14		Extremely-dried	0.0081	63.3	33.5
24		Low air-dried 2	0.031	64.7	37.3
32		Low air-dried 1	0.045	62.9	37.3
28		Low air-dried 2	0.045	63.5	36.4
16		High air-dried	0.16	56.1	39.1
40		High air-dried	0.17	58.3	34.4
13		High air-dried	0.19	57.7	34.3
42		Air-dried for 1 d	0.45	51.6	–
34		Water-saturated	1	52.8	38.1
20		Water-saturated	1	51.3	34.3
36		Water-saturated	1	50.5	32.3

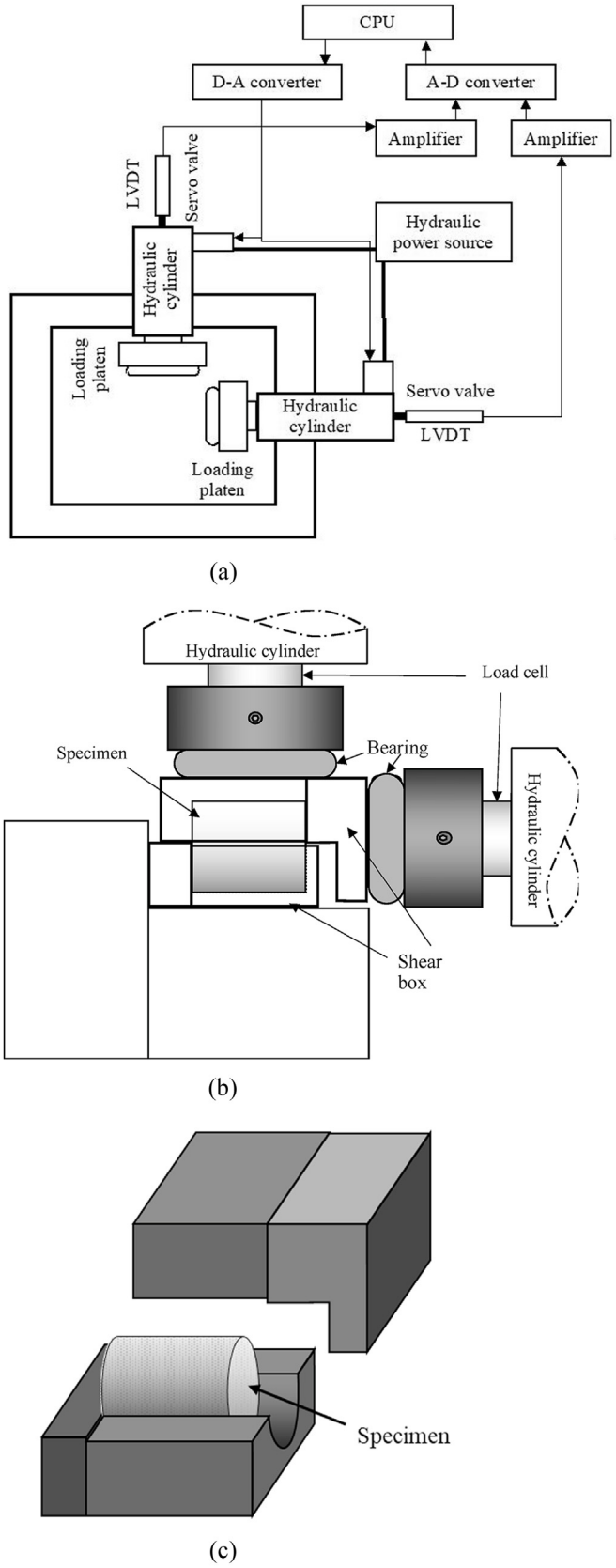

Fig. 2. Testing machine and equipment for the direct shear tests: (a) Schematic of the machine and the control system, (b) Loading part of the machine, and (c) Shear box and specimen.

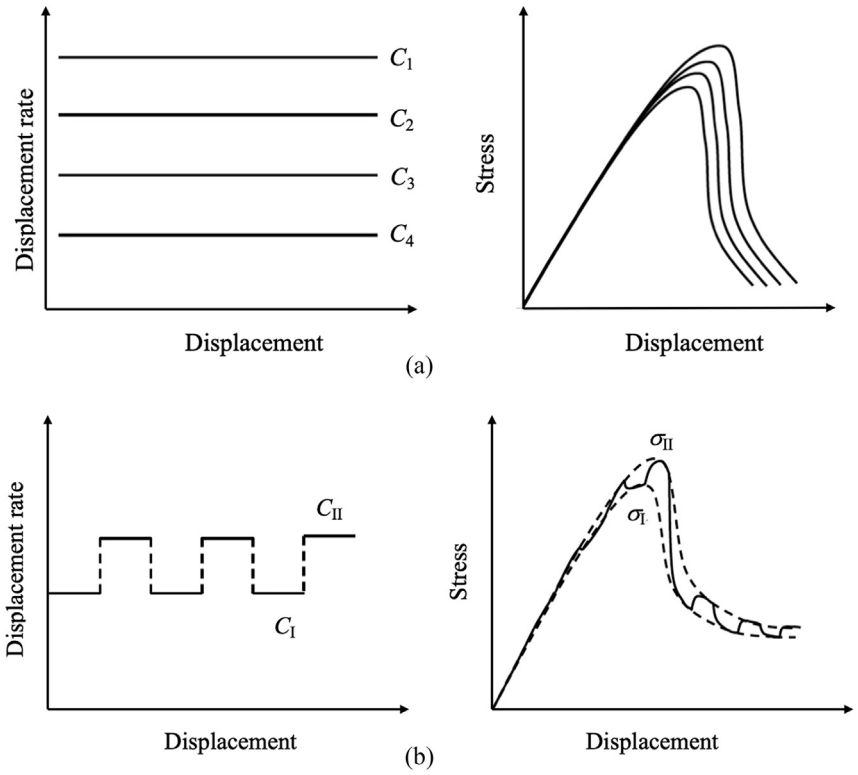

Fig. 3. Two test methods to investigate the loading-rate dependence of rock strength (Okubo et al., 2013): (a) Multi-displacement rate, and (b) Alternating displacement rate between high and low rates.

area for calculating the stress was around 2500 mm^2. The tests were conducted under three vertical stresses: 10 MPa, 25 MPa, and 40 MPa. The horizontal displacement rate varied between the slow rate C_1 (0.005 mm/s) and the rapid rate C_2 (0.05 mm/s) at uniform displacement intervals in a similar manner to the uniaxial compression test proposed by Hashiba et al. (2006). Fig. 3a shows the conventional method, where the horizontal displacement rate is constant during the loading process. Four stress-displacement curves are obtained from the four different tests. In the method shown in Fig. 3b, the horizontal displacement rate changed between two phases of high (C_I) and low (C_{II}) values at the same displacement interval during the loading process, which saves time and the number of specimens (Okubo et al., 2013). Consequently, one specimen can provide two shear strengths (σ_I and σ_{II}) corresponding to the two displacement rates, which are the peak points of envelope curves.

3. Results of direct shear tests

Fig. 4 shows the typical relationship between shear stress and horizontal displacement (hereinafter referred as stress-displacement curves). The shear stress was calculated by dividing the horizontal load by the initial cross-sectional area of the specimen. The stress-displacement curves in Fig. 4a–c are almost straight from the beginning of loading to shear stress of 70%. The effect of alternating displacement rate is hardly observed. The curves are concave downward and obviously fluctuate at shear stress of more than 70%. After the peak points, the curves are concave and fluctuate upwards, and then the stress remains virtually constant, which is known as residual strength. The curves for greater water saturation conditions are situated below the curves for lower water saturation conditions under three vertical stresses. Both the slope of the stress-displacement curve in the pre-peak region and the shear strength are larger for the lower water saturation conditions. As displayed in Fig. 4a–c under vertical stresses of 10 MPa, 25 MPa, and 40 MPa, the displacements at the peak point fall between 0.5 mm and 0.7 mm, between 0.7 mm and 0.9 mm, and between 0.9 mm and 1.1 mm, respectively, in different water saturation conditions. The two envelope curves shown by thin lines in Fig. 4 correspond to the stress-displacement curves at the two displacement rates. These curves are drawn with a spline interpolation by connecting the points at which the displacement rate was changed from C_1 to C_2 or from C_2 to C_1. The displacement-rate dependence of strength can be examined based on the difference between the shear strengths on the envelope curves.

Fig. 5 shows the typical relationship between vertical and horizontal displacements obtained from the same specimens in Fig. 4. The curves are concave upward from the beginning of loading to the inflection point where the fracture surface is probably formed and are then almost straight with a gentle slope. The curves under all the vertical stresses are similar in shape in different water saturation conditions, suggesting that water saturation has a small effect on the vertical displacement. The slope of the curves after the inflection point decreases with the increase of the vertical stress, probably due to the fracture of surface asperities on the failure plane during sliding.

The shear strengths were obtained from the peak points on the lower envelope curves corresponding to the displacement rate of C_1 (0.005 mm/s) in Fig. 4. The residual strengths were determined to be the stresses at a displacement of 2 mm under vertical stress of 10 MPa and 25 MPa and at a displacement of 3 mm under a vertical stress of 40 MPa on the lower envelope curves. These strengths are summarized in Table 2. As the specimens used in this study were shared with other research groups, the specimen numbers shown in Table 2 are irregular. The relationship between these strengths and vertical stress are shown in Fig. 6. Both of the strengths

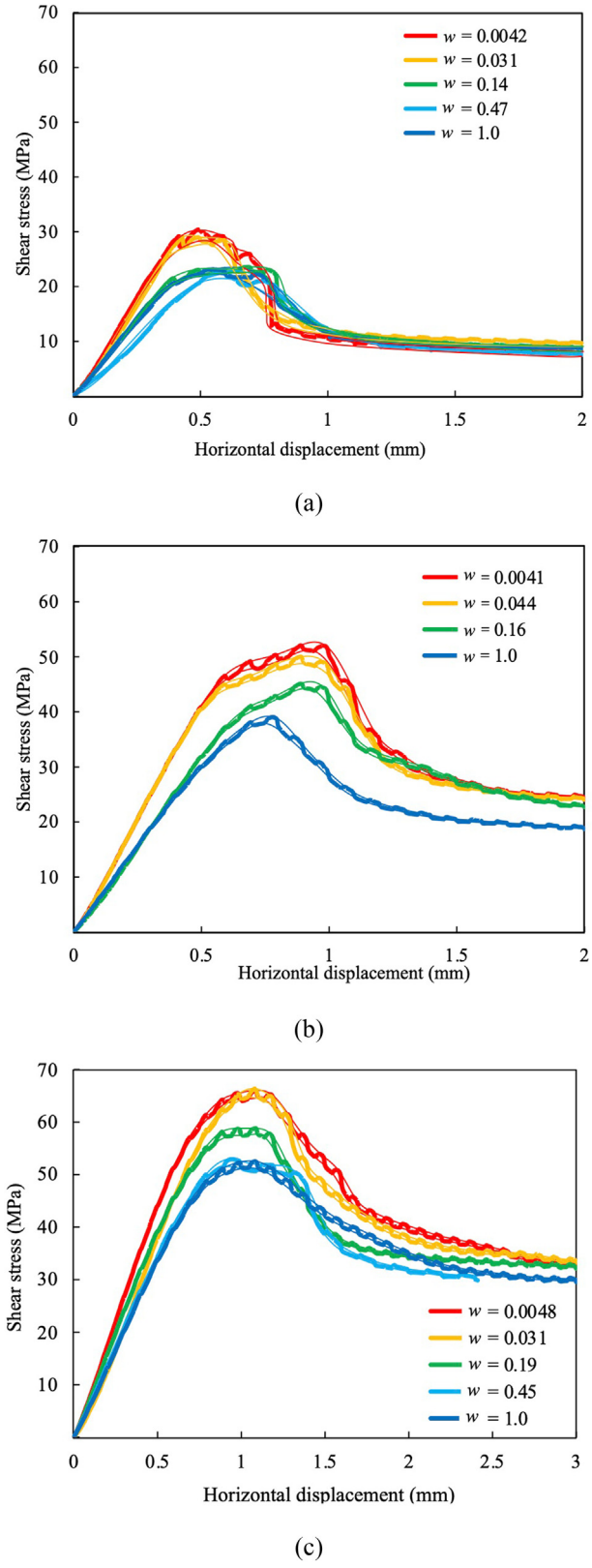

Fig. 4. Stress–displacement curves obtained from the shear tests under vertical stresses of (a) 10 MPa, (b) 25 MPa, and (c) 40 MPa. Thick lines represent the experimental curves, and thin lines represents the envelope curves.

increase with vertical stress. The shear strength has a decreasing trend with increasing water saturation, and in contrast, the residual strength is hardly affected by the water saturation.

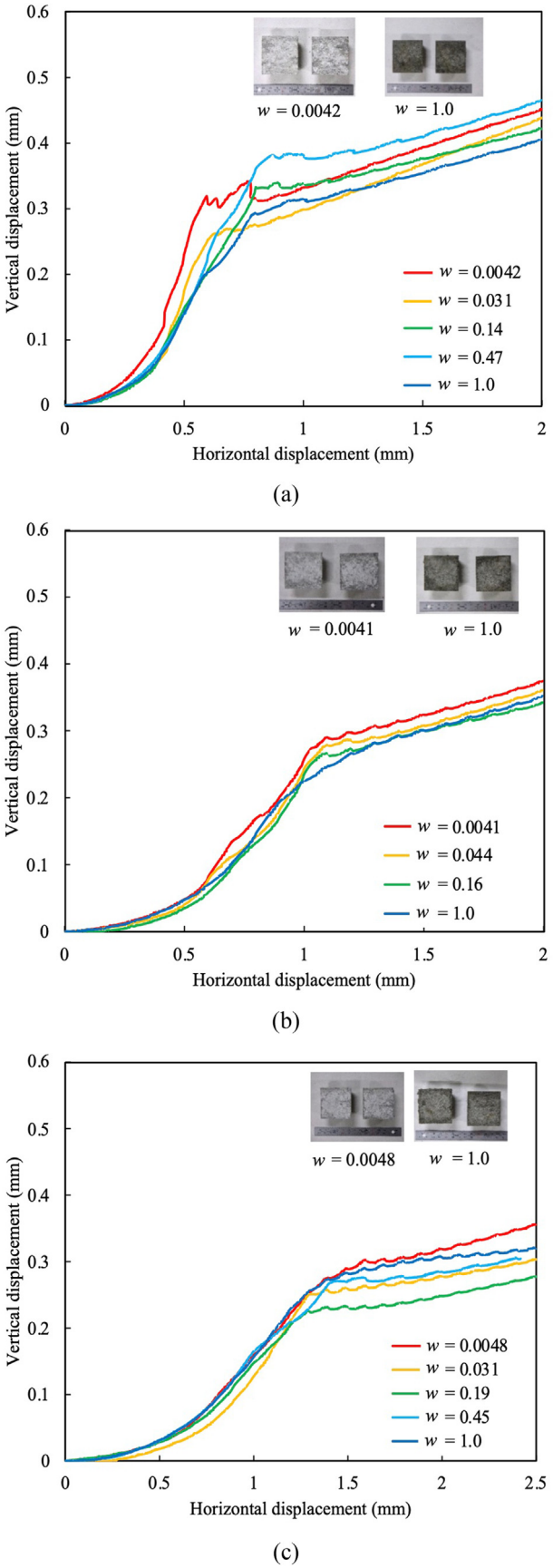

Fig. 5. Vertical displacement–horizontal displacement curves and photographs of failure planes obtained from the shear tests under vertical stresses: (a) 10 MPa, (b) 25 MPa, and (c) 40 MPa.

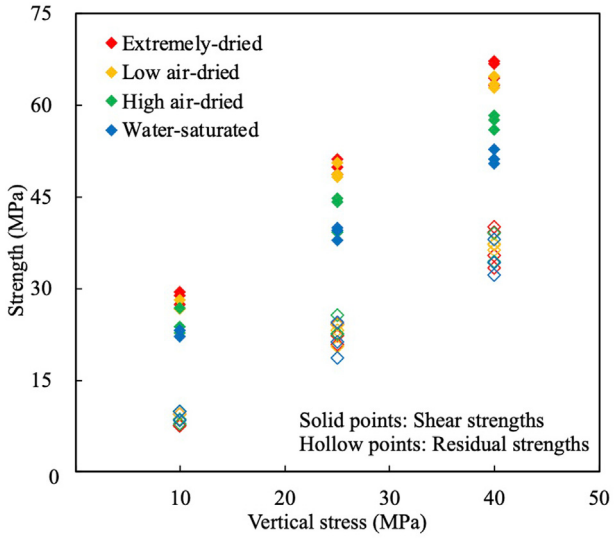

Fig. 6. Relationship between shear and residual strengths and vertical stress.

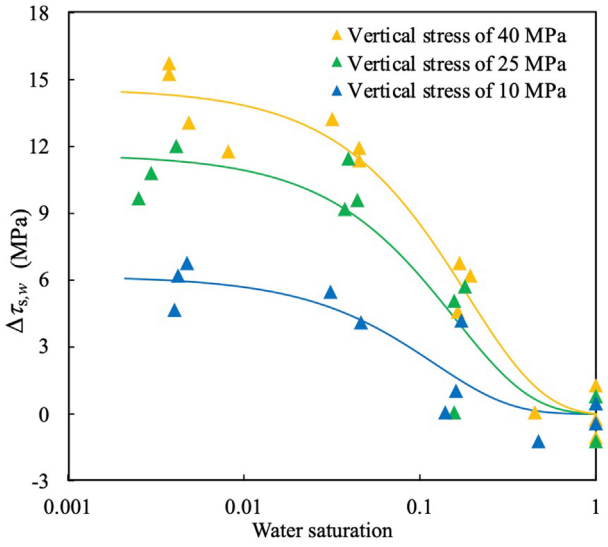

Fig. 8. Relationship between $\Delta\tau_{s,w}$ and water saturation.

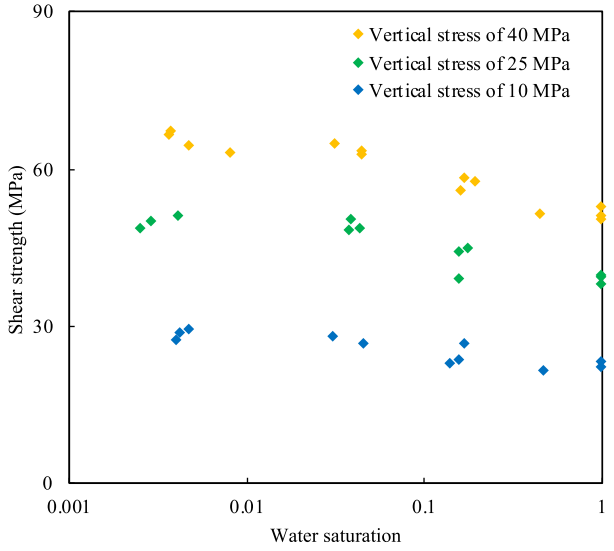

Fig. 7. Relationship between shear strength and water saturation.

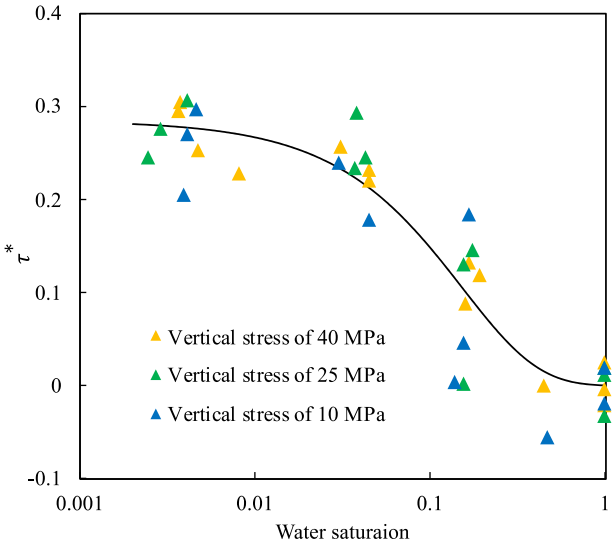

Fig. 9. Relationship between τ^* and water saturation.

The relationship between the shear strength and the logarithm of water saturation is shown in Fig. 7. The shear strength under the three vertical stresses decreases with increasing water saturation. For further investigation of the strength change with water saturation, the difference $\Delta\tau_{s,w}$ in shear strength was calculated by subtracting the average strength of water-saturated specimens from the strength of each specimen under each of the vertical stresses, as shown in Fig. 8. Here, $\Delta\tau_{s,w}$ increases from 0 MPa to 5 MPa, from 0 MPa to 10 MPa, and from 0 MPa to 15 MPa under vertical stresses of 10 MPa, 25 MPa, and 40 MPa, respectively, with decreasing water saturation from 1 to 0.005. In addition, $\Delta\tau_{s,w}$ was divided by the average strength of water-saturated specimens and is shown as τ^* in Fig. 9. Here, τ^* increases with decreasing water saturation, independent of the vertical stress. Yilmaz (2010) listed four regression models of linear, exponential, power, and logarithmic functions for relating uniaxial compressive strength and water content and reported that the exponential function produced the best fit. Hence, this exponential function was applied to the shear strength τ_s obtained in this study as follows:

$$\tau_s = ae^{-bw} + c \tag{2}$$

The following formula for τ^* was derived from Eq. (2):

$$\tau^* = a'\left(e^{-bw} - e^{-b}\right) \tag{3}$$

$$a' = \frac{a}{ae^{-b} + c} \tag{4}$$

As shown by the solid line in Fig. 9, τ^* obtained from the tests is approximated by Eq. (3) with $a' = 0.29$ and $b = 6.5$. The solid lines shown in Fig. 8 are the calculated results obtained by multiplying τ^* by the average strength of water-saturated specimens under each of the vertical stresses, and well coincide with the experimental results.

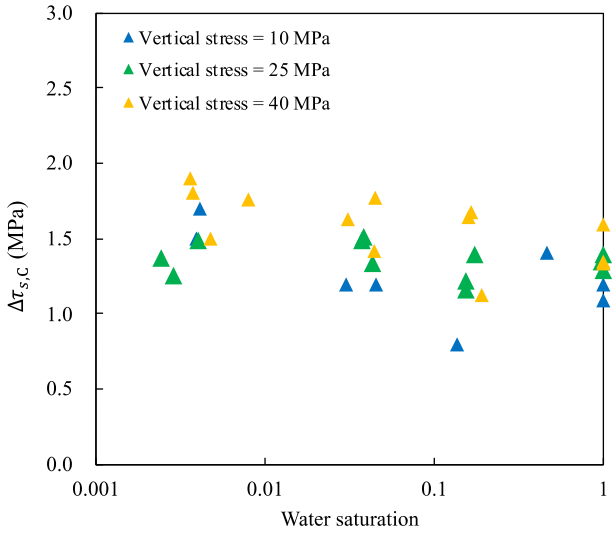

Fig. 10. Relationship between $\Delta\tau_{s,C}$ and water saturation.

The two shear strengths corresponding to the two displacement rates C_1 and C_2 were obtained from the envelope curves, as shown in Fig. 4, and their difference $\Delta\tau_{s,C}$ was calculated by subtracting the strength at C_1 from the strength at C_2 for each of the specimens. The relationship between $\Delta\tau_{s,C}$ and the logarithm of water saturation is shown in Fig. 10. Here, $\Delta\tau_{s,C}$ is almost constant with changing water saturation under each of the vertical stresses of 10 MPa, 25 MPa, and 40 MPa, and the average values are 1.3 MPa, 1.4 MPa, and 1.6 MPa, respectively.

4. Discussion

Hashiba et al. (2019) and Bao et al. (2021) conducted the uniaxial compression tests and Brazilian tension tests, respectively, on Sanjome andesite. In these previous studies, the relationship between strength and water saturation was approximated by the following logarithmic function, which is listed in Yilmaz (2010), as shown in Fig. 11:

$$\sigma_f = p\log_{10}(1/w) + q \tag{5}$$

where σ_f represents the uniaxial compressive strength or the Brazilian tensile strength. Here p, q equal to 8.1 and 71 in Figs. 11a, 2.9 and 4.6 in Fig. 11b, respectively. In contrast, the shear strength was approximated by the exponential function given in Eq. (2) in this study, and the results calculated with the following exponential function for the uniaxial compressive with $a = 22$, $b = 19$, and $c = 81$ and Brazilian tensile strengths with $a = 6.7$, $b = 5.1$, and $c = 4.2$, are also shown in Fig. 11:

$$\sigma_f = ae^{-bw} + c \tag{6}$$

The exponential function was better for approximating the relationship between shear strength and water saturation than the logarithmic function. In contrast, the values of the residual sum of squares are 238 with the logarithmic function and 253 with the exponential function for the uniaxial compressive strength. These values are 44 and 41, respectively, for the Brazilian tensile strength. The degree of approximation was rarely different between the two functions for approximating the relationship between uniaxial

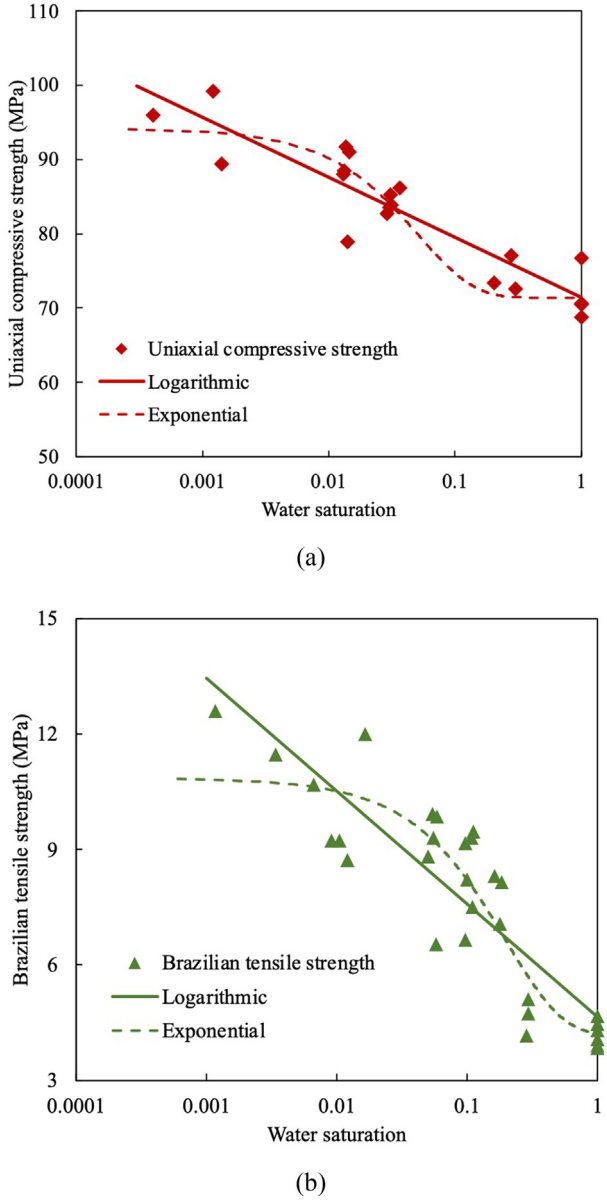

Fig. 11. Relationship between uniaxial compressive and Brazilian tensile strengths and water saturation: (a) Uniaxial compressive strength (Hashiba et al., 2019), and (b) Brazilian tensile strength (Bao et al., 2021).

compressive and Brazilian tensile strengths and water saturation. However, the exponential function seems to be better, because the strength approaches constant values at a water saturation of 1 in extremely low water saturation condition.

The blue, green, and red squares in Fig. 12 indicate the shear strengths calculated by Eq. (2) for water saturations of 1, 0.1, and 0.01, respectively. The mechanical properties of the Sanjome andesite specimens utilized for shear tests in this study are close to those of the specimens used for the Brazilian tensile tests in Bao et al. (2021), as shown in Table 1. Hence, the Mohr's circles for water saturation of 1, 0.1, and 0.01 are drawn in blue, green, and red, respectively, using the Brazilian tensile strengths calculated by Eq. (6) with $a = 6.7$, $b = 5$, and $c = 4.2$. Then, the Hoek-Brown failure envelopes are drawn by the blue, green, and red broken lines to pass the shear strengths and to contact the circles in each of the water saturation conditions. The Hoek-Brown failure criterion is

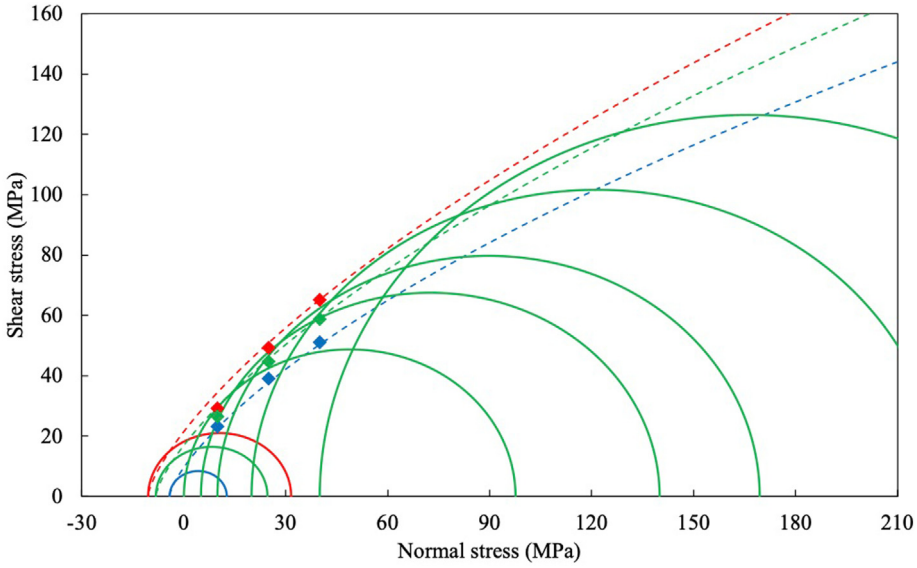

Fig. 12. Shear strength, Mohr's circles, and Hoek-Brown failure envelopes under the three water saturation conditions. Red, green and blue data points stand for the shear strengths obtained in this study under $w = 0.01$, 0.1 and 1, respectively. Red and blue circles represent the Mohr's circles obtained from Brazilian tension test while green circles denote the Mohr's circles obtained from the uniaxial compression test. Red, green and blue dashed curves are the envelopes of the Mohr's circles corresponding to $w = 0.01$, 0.1 and 1, respectively.

represented with the principal stresses as follows and is converted to the failure envelope on the shear and normal stress diagram (Eberhardt, 2012):

$$\sigma_1 = \sigma_3 + \sigma_c\left(m\frac{\sigma_3}{\sigma_c} + 1\right)^{0.5} \tag{7}$$

$$m = \frac{Br^2 - 1}{Br} \tag{8}$$

where σ_1 and σ_3 are the maximum and minimum principal stresses, respectively; and σ_c is the uniaxial compressive strength; m is a variable in this failure criterion; Br is the ratio of the uniaxial compressive to tensile strength, which is known as the brittleness index.

Okubo et al. (1990) conducted triaxial compression tests under air-dried conditions on Sanjome andesite specimens for which unconfined strengths are close to those of the specimens used in this study, as shown in Table 1. Although the water saturation of the specimens used for these triaxial compression tests is unknown, the Mohr's circles for the triaxial compressive strengths are drawn in Fig. 12. The failure envelope in green obtained from the shear and Brazilian strengths at a water saturation of 0.1, which corresponds to the air-dried condition, also seems to be the failure envelope for the Mohr's circles obtained from the triaxial compressive strengths in air-dried conditions. The failure envelopes in higher water saturation conditions are situated beneath the failure envelopes in lower water saturation conditions, which indicates that the triaxial compressive strengths as well as the unconfined strengths are lower in higher water saturation conditions. Meanwhile, the failure envelope for a water saturation of 0.1 is located closer to that for 0.01 than that for 1, which indicates that rock failure is less affected by water under lower water saturation conditions. The values of m in Eq. (7) are 12, 12, and 14 for water saturations of 0.01, 0.1, and 1, respectively, which indicates that Br is almost constant, independent of water saturation.

The green squares in Fig. 13b are the same as those in Fig. 12. The increase $\Delta\tau_{s,C}$ in shear strength with a tenfold increase of displacement rate was found to be 1.3 MPa, 1.4 MPa, and 1.6 MPa under vertical stresses of 10 MPa, 25 MPa, and 40 MPa, respectively, as shown in Fig. 10. Hence, the shear strengths at a hundredfold displacement rate (0.5 mm/s) and at a one hundredth displacement rate (0.00005 mm/s) were calculated with $2\Delta\tau_{s,C}$ and are shown by red and blue squares in Fig. 13a and c, respectively. The smallest green circle in Fig. 13b is the same as that in Fig. 12 obtained from the Brazilian tensile strength at a displacement rate of 0.005 mm/s. The other green circles in Fig. 13b are the same as those in Fig. 12 obtained from the triaxial compressive strengths at a strain rate of 10^{-4} s^{-1}, where the test duration is similar to that for the shear tests in this study. In previous studies, the relationship between the compressive and tensile strengths σ_f and loading rate C were represented by the following formula:

$$\sigma_f \propto C^{\frac{1}{n+1}} \tag{9}$$

where n is a constant representing the degree of loading-rate dependence. The value of n is around 38 in uniaxial compression and tension and increases with increasing confining pressure in triaxial compression, as reported by Okubo et al. (1990). The Mohr's circles are drawn in red and blue in Fig. 13a and c using the strengths calculated by Eq. (9) at the hundredfold loading rate and that at hundredth loading rate, respectively. Then, the Hoek-Brown failure envelopes are drawn to pass the shear strengths and to contact the circle for the Brazilian tensile strength in each of the water saturation conditions in the same manner as Fig. 12. The failure envelopes in the three colors obtained from the shear and Brazilian strengths at the three loading rates also seem to be the failure envelopes for the Mohr's circles obtained from the triaxial compressive strengths. The values of m are the same (12) at the slow, medium, and fast loading rates, which indicates that Br is independent of not only the water saturation but also the loading rate.

Assuming that Br or m in Eq. (8) is constant for Sanjome andesite, the Hoek-Brown failure criterion is determined by either the uniaxial compressive or tensile strength that depends on both the water saturation and the loading rate. The change of uniaxial compressive strength with the change of water saturation and loading rate is represented by Eqs. (6) and (9), respectively. Hence, the influences of water saturation and loading rate can be

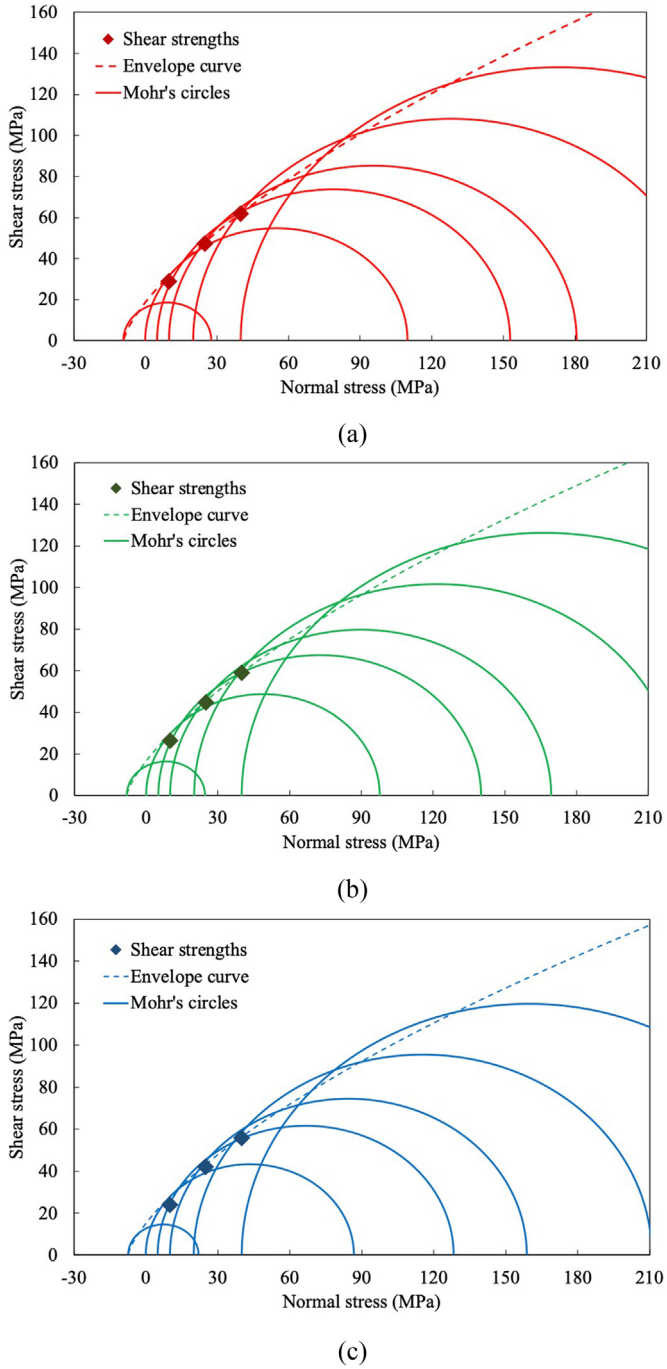

Fig. 13. Shear strength, Mohr's circles, and Hoek-Brown failure envelopes at the three loading rates: (a) Displacement rate of 0.5 mm/s in the shear and Brazilian tension tests, and strain rate of 10^{-2} s^{-1} in the triaxial compression tests; (b) Displacement rate of 0.005 mm/s in the shear and Brazilian tension tests, and strain rate of 10^{-4} s^{-1} in the triaxial compression tests; and (c) Displacement rate of 0.00005 mm/s in the shear and Brazilian tension tests, and strain rate of 10^{-6} s^{-1} in the triaxial compression tests.

converted as shown in Fig. 14. The curve in this figure indicates the relationship between water saturation and loading rate that generates the same strength change. For example, the strength increases from the water saturation of 1 to 0.001 is equivalent to the strength increase with a 4×10^4-times increase of loading rate. This result indicates that the Hoek-Brown failure envelopes can be drawn for an arbitrary water saturation and loading rate using this curve and a single set of strength and brittleness index *Br*.

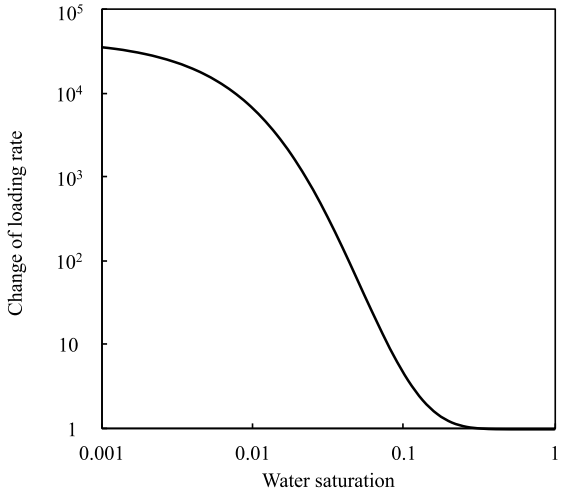

Fig. 14. Relationship between water saturation and loading rate generating the same strength change of Sanjome andesite.

5. Conclusions

Sanjome andesite was subjected to direct shear tests under five water saturation conditions. The tests were conducted under three vertical stresses at different horizontal displacement rates. The horizontal stress–horizontal displacement curves in greater water saturation levels were situated below the curves in lower water saturation levels under each of the three vertical stresses, and, in contrast, the vertical displacement–horizontal displacement curves under each of the vertical stresses were similar in shape under different water saturation conditions. Both the shear and residual strengths showed an almost linearly increasing trend with increasing vertical stress. Although the residual strength was hardly affected by the water saturation, the shear strength decreased with increasing water saturation and was approximated by an exponential function. It was likewise tracked down that the increment in shear strength with a tenfold increase in displacement rate is practically consistent under each of the vertical stresses.

The authors applied the exponential function representing the shear strength and water saturation to the uniaxial compressive and Brazilian tensile strengths in the previous studies and then showed the effect of water saturation on the Hoek-Brown failure criterion for the andesite. In addition, based on the loading rate dependence of shear, compressive, and tensile strengths, the effect of loading rate on the Hoek-Brown failure criterion for the andesite was also discussed. These results indicated that the brittleness index of the andesite, which is defined as the ratio of uniaxial compressive strength to tensile strength, is independent of not only water saturation but also loading rate, and that the effects of the water saturation dependence and the loading rate dependence of the failure criterion can be converted between each other. The future step in this research is to collect data on the influences of water saturation and loading rate under the triaxial stress state for validating the results in this study and to collect data for rocks other than the andesite used in this study.

Declaration of competing interest

The authors declare that they have no known competing financial interests or personal relationships that could have appeared to influence the work reported in this paper.

Acknowledgments

The authors are grateful to Mr. Shengyu Zang of the University of Tokyo for his assistance in conducting the tests.

References

Bao, T., Hashiba, K., Fukui, K., 2021. Effect of water saturation on the Brazilian tension test of rocks. Mater. Trans. 62 (1), 48–56.
Brace, W.F., Martin III, R.J., 1968. A test of the law of effective stress for crystalline rocks of low porosity. Int. J. Rock Mech. Min. Sci. Geomech. Abstr. 5 (5), 415–426.
Dyke, C.G., Dobereiner, L., 1991. Evaluating the strength and deformability of sandstones. Q. J. Eng. Geol. Hydrogeol. 24 (6), 123–134.
Eberhardt, E., 2012. The Hoek–Brown failure criterion. Rock Mech. Rock Eng. 45 (6), 981–988.
Erguler, Z.A., Ulusay, R., 2009. Water-induced variations in mechanical properties of clay-bearing rocks. Int. J. Rock Mech. Min. Sci. 46 (2), 355–370.
Fukui, K., Okubo, S., Iwano, K., 2003. Loading rate dependency of Sanjome andesite and Tage tuff in uniaxial tension. Journal of JSCE 729, 59–71 (in Japanese).
Fukui, K., Okubo, S., Ogawa, A., 2004. Some aspects of loading-rate dependency of Sanjome andesite shear strength. Int. J. Rock Mech. Min. Sci. 41 (7), 1215–1219.
Gunsallus, K.T., Kulhawy, F.H., 1984. A comparative evaluation of rock strength measures. Int. J. Rock Mech. Min. Sci. Geomech. Abstr. 21 (5), 233–248.
Gutierrez, M., Øino, L.E., HØeg, K., 2000. The effect of fluid content on the mechanical behaviour of fractures in chalk. Rock Mech. Rock Eng. 33 (2), 93–117.
Hashiba, K., Okubo, S., Fukui, K., 2006. A new testing method for investigating the loading rate dependency of peak and residual rock strength. Int. J. Rock Mech. Min. Sci. 43 (6), 894–904.
Hashiba, K., Fukui, K., 2015. Effect of water on the deformation and failure of rock in uniaxial tension. Rock Mech. Rock Eng. 48 (5), 1751–1761.
Hashiba, K., Fukui, K., Kataoka, M., Chu, S.Y., 2018. Effect of water on the strength and creep lifetime of andesite. Int. J. Rock Mech. Min. Sci. 108, 37–42.
Hashiba, K., Fukui, K., Kataoka, M., 2019. Effects of water saturation on the strength and loading-rate dependence of andesite. Int. J. Rock Mech. Min. Sci. 117, 142–149.
Hawkes, I., Mellor, M., Gariepy, S., 1973. Deformation of rocks under uniaxial tension. Int. J. Rock Mech. Min. Sci. Geomech. Abstr. 10 (6), 493–507.
Kim, T., Jeon, S., 2019. Experimental study on shear behavior of a rock discontinuity under various thermal, hydraulic and mechanical conditions. Rock Mech. Rock Eng. 52, 2207–2226.
Kirby, S.H., 1984. Introduction and digest to the special issue on chemical effects of water on the deformation and strengths of rocks. J. Geophys. Res.: Solid Earth. 89 (B6), 3991–3995.
Li, Z., Sheng, Y., Reddish, D.J., 2005. Rock strength reduction and its potential environmental consequences as a result of groundwater rebound. In: Proceeding of 9th International Mine Water Congress. Oviedo, Asturias, Spain, pp. 513–519.
Ojo, O., Brook, N., 1990. The effect of moisture on some mechanical properties of rock. Min. Sci. Technol. 10 (2), 145–156.
Okubo, S., Nishimatsu, Y., He, C., 1990. Loading rate dependence of class II rock behaviour in uniaxial and triaxial compression tests–an application of a proposed new control method. Int. J. Rock Mech. Min. Sci. 27 (6), 559–562.
Okubo, S., Hashiba, K., Fukui, K., 2013. Loading rate dependency of the strengths of some Japanese rocks. Int. J. Rock Mech. Min. Sci. 58, 180–185.
Pellet, F.L., Keshavarz, M., Boulon, M., 2013. Influence of humidity conditions on shear strength of clay rock discontinuities. Eng. Geol. 157, 33–38.
Peng, S.S., 1973. Time-dependent aspects of rock behavior as measured by a servocontrolled hydraulic testing machine. Int. J. Rock Mech. Min. Sci. Geomech. Abstr. 10 (3), 235–246.
Talesnick, M.L., Hatzor, Y.H., Tsesarsky, M., 2001. The elastic deformability and strength of a high porosity, anisotropic chalk. Int. J. Rock Mech. Min. Sci. 38 (4), 543–555.
Talesnick, M.L., Shehadeh, S., 2007. The effect of water content on the mechanical response of a high-porosity chalk. Int. J. Rock Mech. Min. Sci. 44 (4), 584–600.
Ulusay, R., Karakul, H., 2016. Assessment of basic friction angles of various rock types from Turkey under dry, wet and submerged conditions and some considerations on tilt testing. Bull. Eng. Geol. Environ. 75 (4), 1683–1699.
Vásárhelyi, B., Ván, P., 2006. Influence of water content on the strength of rock. Eng. Geol. 84 (1–2), 70–74.
Yilmaz, I., 2010. Influence of water content on the strength and deformability of gypsum. Int. J. Rock Mech. Min. Sci. 47 (2), 342–347.

Tianshu Bao obtained his MSc and PhD degrees in Systems Innovation from the University of Tokyo in Graduate School of Engineering. His research interests include: (1) energy extraction, (2) the stability of underground spaces, and (3) moisture damage properties of rock.